COMPARATIVE ANALYSIS OF RNG k-ε AND 'STANDARD' k-ε MODELS FOR FLUID FLOW AROUND A CYLINDER

A. K. Temu
Department of Chemical and Process Engineering,, University of Dar Es Salaam,
P. O. Box 35131, Dar Es Salaam, Tanzania

Abstract

A two-dimensional computational scheme for simulating fluid flow around a cylinder was investigated. RNG (**Re-Normalisation Group**) and 'standard' k-ε turbulent closure models were used. The simulation was implemented with assistance of FLOW-3D computational fluid dynamics (CFD) code. The governing equation of fluid motion, in Eulerian form, included body forces as well as surface forces. The computational model predictions for fluid velocity showed good agreement between the two models. Comparison of the viscosities showed a large deviation from the two models, with RNG k-ε model giving a better approximation. Comparison of the velocity around the cylinder, as obtained from RNG k-ε model, with approximation method for laminar boundary layer on the front part of the cylinder showed a very good agreement reflecting the effect of blockage.

Keywords: *turbulence, cross-flow, CFD, RNG, cylinder*

INTRODUCTION

There is a close relation between the dynamics of flow over a cylinder and heat and mass transfer characteristics of a system. Studies of such dynamic processes as pressure distribution, variation of free stream velocity, and friction drag, are needed to achieve a proper understanding of these relations. The effect of free stream turbulence and that of shell - channel blockage are also important. Each of these processes influences in some way, the fluid dynamics on the surface, the separation of the boundary layer, and the formation of the wake.

In addressing the issues of turbulent closure and time accuracy, promises of Direct Numerical Simulation (DNS) where all of the relevant lengths scales are resolved with highly refined meshes, and Large Eddy Simulations (LES), where the smallest length scales are modelled are yet to be realised [1]. Therefore, turbulence modelling based on Navier - Stokes equations is used to approximate the effects of turbulence on the mean flow.

Turbulent models used in industrial flow computation fall into two general categories, viz. eddy viscosity models and stress transport models. The eddy viscosity models are based on the hypothesis that the effect of turbulence can be mimicked through an additional viscosity, the eddy viscosity that augments the molecular viscosity. A variety of two-equation models have been proposed. These differ in accuracy and suitability for application in different flow geometries. It is, therefore, the objective of this work to compare the suitability of RNG k-ε against that of 'standard' k-ε model for flow perpendicular to a cylinder.

GOVERNING EQUATIONS

Because the fluid in this investigation had Mach numbers less than 0.2, it was considered incompressible. For incompressible fluid in turbulent flow, the averaged governing equations are:

$$\frac{\partial \bar{u}_j}{\partial x_j} = 0 \qquad (1)$$

$$\frac{\partial \bar{u}_i}{\partial t} + u_j \cdot \frac{\partial \bar{u}_i}{\partial x_j} = -\frac{1}{\rho} \cdot \frac{\partial \bar{p}}{\partial x_i} + \nu \cdot \frac{\partial}{\partial x_j}\left(\frac{\partial \bar{u}_i}{\partial x_j} + \frac{\partial \bar{u}_j}{\partial x_i}\right) - \frac{\partial}{\partial x_j}\left(\overline{u'_j u'_i}\right) + g_i \qquad (2)$$

where $\overline{u}$ is the mean velocity and u′ is the fluctuating component $(u = \overline{u} + u')$. The double covariance $\overline{u_i' u_j'}$ is the turbulent Reynolds stresses. The most common method of approximate turbulence closure is:

$$\overline{u_i' u_j'} = -\nu_T \cdot \left(\frac{\partial \overline{u}_i}{\partial x_j} + \frac{\partial \overline{u}_j}{\partial x_i} \right) + \frac{2}{3} \cdot k \cdot \delta_{ij} \qquad (3)$$

where k $\left[= 0.5 \cdot \left(\overline{u_i'^2} + \overline{u_j'^2} + \overline{u_k'^2} \right) \right]$ is the turbulent kinetic energy, δ_{ij} is the Kronecker delta (δ_{ij} = 1 if i = j otherwise equals zero) and ν_T is the eddy viscosity given by:

$$\nu_T = C_\mu \cdot \frac{k^2}{\varepsilon} \qquad (4)$$

where C_μ is an empirical constant and ε is the turbulent dissipation rate.

Incompressible fluids and isochoric flows, as assumed in this work, are very common in engineering applications. All fluids, however, are compressible to a greater or lesser extent. By assuming that the density is constant, the incompressibility conditions represents an idealisation of the physical behaviour of fluids for certain flow conditions and thermodynamic states. This idealisation assumes that any density perturbation due to either pressure or temperature variation is negligible.

When heat is added to or removed from a fluid and density varies with temperature, flow can be induced due to the force of gravity acting on the density variation. That type of flow is termed natural convection and is expressed by the buoyancy term. Use of this expression violates incompressibility condition of constant density. However, the violation is accepted if the density variations are sufficiently small to induce only buoyancy forces

Turbulence Modelling

Two-equation models are more popular methods for turbulence closure. Among them, the 'standard' k-ε model uses two transport equations to calculate both turbulent kinetic energy k and the dissipation rate ε. Once both k and ε are found, the eddy viscosity ν_T is determined by the Prandtl-Kolmogorov relation – Eq. (4).

The models can be categorised by the range of turbulence intensity they are designed for. The parameter characteristic of turbulence level is the dimensionless eddy viscosity defined by:

$$\varepsilon^+ = \frac{\nu_T}{\nu_{mol}} \qquad (5)$$

where ν_{mol} is the molecular viscosity of the fluid.

For laminar flow $\nu_T \equiv 0$, by definition, therefore ε^+ is zero. For fully turbulent incompressible boundary layer flow, ε^+ will vary smoothly from zero at the solid wall to about 500 in the fully turbulent region.

Higher Reynolds number k-ε models do not resolve the low Reynolds number regions near the boundaries. Instead low Reynolds number k-ε models have been developed to include the viscous sublayer in the computational domain through the use of special wall-proximity functions. Example of such models is that of Lam and Bremhorst [2].

Turbulence isotropy in the flow is another factor contributing towards heat and mass transfer. The turbulence is considered isotropic if $0.6 < u'^2/v'^2 < 1.4$ [3]. For practical systems, i.e. Re > 40, this condition is never satisfied at the stagnation point and after the separation point. Therefore, crossflow over a cylinder is anisotropic.

A 'standard' k-ε model assumes that turbulence is isotropic, which in turn, would make dispersion of particle in absence of gravity also isotropic. The k-ε closure, therefore, does not provide adequate turbulence information for anisotropic flow [4,5].

Like the 'standard' k-ε model, RNG (**Re-Normalisation Group**) k-ε model assumes turbulence isotropy. However, it is based on removal of small-scale turbulence by defining dynamic equations for large-scales, averaging them over an infinite band of small-scales. This means it cannot be used with damping equations for low Reynolds numbers like those by Lam and Bremhorst [2]. RNG model

modifies the ε equation leading into better approximations for k and ε [6,7]. It is thus more suitable where anisotropy is involved.

The high Reynolds number form of the RNG k-ε model is given by:

$$\frac{\partial k}{\partial t} + u_j \cdot \frac{\partial k}{\partial x_j} = \nu_T \cdot S^2 - \varepsilon + \nabla \alpha_k \cdot \nu \cdot \nabla k \qquad (6)$$

and

$$\frac{\partial \varepsilon}{\partial t} + u_j \cdot \frac{\partial \varepsilon}{\partial x_j} = C_{\varepsilon 1} \cdot \frac{\varepsilon}{k} \cdot \nu_T \cdot S^2 - C_{\varepsilon 2} \cdot \frac{\varepsilon^2}{k} - R + \nabla \alpha_\varepsilon \cdot \nu \cdot \nabla \varepsilon \qquad (7)$$

where ν ($= \nu_{mol} + \nu_T$) is the total viscosity, $\alpha_k = \alpha_\varepsilon$ are inverse turbulent Prandtl numbers, $C_{\varepsilon 1}$ and $C_{\varepsilon 2}$ are coefficients of production and decay respectively, S^2 ($= 2S_{ij} \cdot S_{ij}$) is the magnitude of the rate of strain and S_{ij} is the mean strain expressed as:

$$S_{ij} = \frac{1}{2} \cdot \left(\frac{\partial u_i}{\partial x_j} + \frac{\partial u_j}{\partial x_i} \right) \qquad (8)$$

The production of dissipation term R is given by:

$$R = \frac{C_\mu \cdot \eta^3 \cdot (1 - \eta/\eta_o)}{1 + \beta \cdot \eta^3} \cdot \frac{\varepsilon^2}{k} \qquad (9)$$

where η ($= S \cdot k/\varepsilon$) is the ratio of the turbulence time scale to the mean strain time scale which is equal to zero in isotropic turbulence and very large in the region of rapid distortion, η_o ($= 4.38$) is the fixed point value of η obtained in the limit of small S_{ij} (that is homogeneous shear flow), and β is a constant related to von Karman constant ($\kappa = 0.4$). In applications β varies between 0.01 and 0.015 with only a small change in κ.

The high Reynolds number form of the 'standard' k-ε model is the same as Eqs. (6) and (7) without R. The RNG theory give values of the constants $C_\mu = 0.085$, $C_{\varepsilon 1} \approx 1.42$, $C_{\varepsilon 2} \approx 1.68$ and $\alpha_k = \alpha_\varepsilon \approx 1.39$, whereas the 'standard' k-ε model gives $C_\mu = 0.090$, $C_{\varepsilon 1} \approx 1.4$, $C_{\varepsilon 2} \approx 1.9$ and $\alpha_k = \alpha_\varepsilon \approx 1$.

The contribution of R in Equation (7) is small for weakly strained turbulence and large in the rapid distortion limit when $\eta \rightarrow \infty$. The reduced value of $C_{\varepsilon 2}$ in the RNG theory has the consequence of decreasing both the rate of production of k and the rate of dissipation of ε, leading to smaller values of ν_T. In the regions of small strain rate, the R tends to increase ν_T somewhat, but it is still typically smaller than its value in the standard theory. However, in the regions of large strain rate, the sign of R is changed and ν_T is decreased even more. This feature of RNG equations is due to the strong anisotropy in the regions of large shear and is responsible for some of the marked improvement of the RNG model in the treatment of flow separation and anisotropic large scale eddies [6].

Near Wall Behaviour

In a turbulent flow the velocity near the wall is "laminar" and its profile is approximated by the law-of-the-wall. Using logarithmic law to estimate shear stress needs a lot of computer time for integration of the momentum thickness. Alternatively, a relatively easy to work with mathematically, one-seventh (1/7)-power law is used. This was expressed as:

$$\frac{u(y')}{U(x')} = \left(\frac{y'}{\delta(x')} \right)^{\frac{1}{7}} \qquad (10)$$

Although power law provide a reasonable approximation to measured velocity profiles across most pipes, it is not valid at the wall surface ($y' = 0$) where the velocity gradient is infinity and at the edge of the boundary layer thickness ($y' = \delta$) where the velocity gradient is non-zero.

While the duct flow might be turbulent, the viscous interaction of the fluid and the obstructing tube surface in cross-flow could give rise to a different boundary layer flow. Factors that determine the fluid dynamics in the boundary layer are the Reynolds number and the free stream turbulence. Most engineering flows across obstructions are in the range $10^3 < Re < 2 \cdot 10^5$. In this range, there exists a steady laminar boundary layer, which persist up to the separation point. The velocity profile in this region then could be more accurately estimated by laminar boundary layer theory. Beyond the separation point the flow pattern is not well defined, but it is assumed to be turbulent and law-of-the-wall theory could be employed.

The separation of boundary layer is governed by friction and changes in the velocity and

pressure. On the front part of the cylinder, the energy of compression of the fluid is transferred to kinetic energy. A reverse transformation occurs at the rear. At the point of separation, velocity gradient normal to the wall vanishes. The structure of the flow field past a circular cylinder is completely different for inviscid fluid than it is for a viscous fluid. This is due to boundary layer separation. Because of boundary layer separation, the average pressure on the rear half of the cylinder is considerably less than that on the front half. Thus a large pressure drag is developed, even though the viscous shear drag may be quite small.

There is no dividing line between the potential flow region, where friction is negligible, and the boundary layer region, because the velocity component parallel to the surface approaches the free stream value u_∞ asymptotically. Customarily, however, the boundary layer is defined as the region where the velocity component parallel to the surface is less than 99 per cent of the free stream velocity.

Location of the point of separation is determined by integration of the boundary layer equation. However, approximation methods by Thwaites, von Karman and Pohlhausen, and Holstein and Bohlen are much simpler [8,9]. The location of this separation point is also slightly influenced by the blockage factor b_f (= D/H where D is the cylinder diameter and H is the channel width) of the system [10]. Also affected by the blockage factor is the boundary layer thickness.

According to Schlichting [8] the tangential velocity on the front part of a cylinder at distance x' from the stagnation point and distance y' from the wall is approximated as:

$$\frac{u(y)}{U(x)} = \left(2\cdot\eta - 2\cdot\eta^2 + \eta^4\right) + \frac{\Lambda}{6}\cdot\left(\eta - 3\cdot\eta^2 + 3\cdot\eta^3 - \eta^4\right) \quad (11)$$

where dimensionless distance from the wall η and the shape factor Λ are related to the local boundary layer thickness $\delta(x')$.

Incorporating the blockage effect, Zukauskas and Ziugzda [10] expressed the free stream tangential velocity U (x) at position x along the surface as:

$$U(x') = u_\infty \cdot \left(a_1 \cdot \left(\frac{x'}{D}\right) + a_3 \cdot \left(\frac{x'}{D}\right)^3 + a_5 \cdot \left(\frac{x'}{D}\right)^5\right) \quad (12)$$

where a_1, a_2, a_3 are constants given by:

$$a_1 = 3.6314 \cdot \left(1 + \frac{b_f}{2}\right) \quad (13a)$$

$$a_3 = -2.1709 \cdot \left(1 - 12.1284 \cdot {b_f}^{2.226} + 3.7376 \cdot b_f\right) \quad (13b)$$

$$a_5 = -1.5144 \cdot \left(1 + 18.542 \cdot {b_f}^{2.277} - 6.878 \cdot b_f\right) \quad (13c)$$

From the definition of the viscous shear stress at the wall we get the velocity gradient, which is expressed as:

$$\left(\frac{du}{dy'}\right)_{y'=0} = \left(2 + \frac{\Lambda}{6}\right) \cdot \frac{U(x')}{\delta(x')} \quad (14)$$

Beyond the boundary layer separation point, the wall shear stress remains close to zero up to the rear stagnation point [10]. In this region there is no steady state boundary layer, and complex vortices are formed in the wake. This transition is characterised by a sharp decrease in the pressure drag, a high rarefaction at the back of the cylinder, and irregular vortex shedding. The flow in this region is essentially turbulent and the above boundary layer estimates are invalid.

Vortices circulate in a stationary position or are regularly shed from the cylinder and form the so-called vortex street. The Re, the free stream turbulence, the blockage factor, and the nature of the surface govern their behaviour. For Re between 3.10^2 and 2.10^5, the vortex shedding is regular and occupies about 50 diameters from the cylinder and the wake becomes fully turbulent [10]. Regular vortex shedding provides a constant exchange of mass, momentum, and energy between the vortex wake and the free stream.

IMPLEMENTATION OF THE MODEL

The governing equations were solved using Flow-3D code. Flow-3D code is a multi purpose, commercial, software for analysis of fluid dynamics and thermal phenomena. The difference equations in Flow-3D are based on a fixed Eulerian mesh of non-uniform rectangular control volumes using the **F**ractional **A**rea/**V**olume **O**bstacle **R**epresentation (FAVOR) method.

The finite difference mesh used for numerically solving the governing equations consists of rectangular cells. The active mesh region is surrounded by layers of fictitious or boundary cells used to set mesh boundary conditions. With each cell there are associated local average values of all dependent variables. The velocity components and the fractional areas are located at the centre of the cell faces. All other variables like pressure, fluid fraction, densities, internal energies and viscosities are located at the centre of the cells. The time-step size is restricted to avoid numerical instabilities. Because the flow fields were observed to be symmetrical only one half of the duct was used in the simulations. Figure 1 shows the computational mesh for the flow around a cylinder.

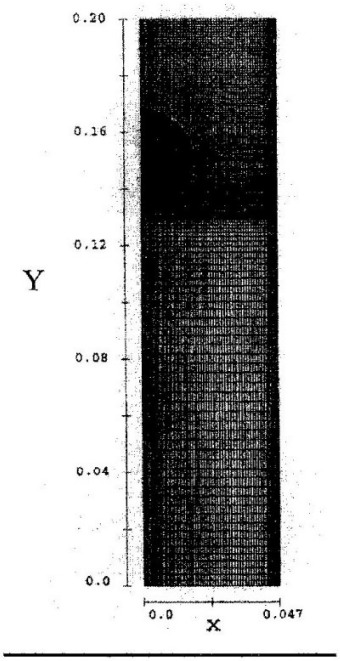

Figure 1. Computational mesh for crossflow around a cylinder

DISCUSSION OF RESULTS

Simulations were run for airflow through a channel of cross-section 0.1m x 0.2m. A cylindrical obstruction of diameter 0.036m and length 0.2m ran across the channel resulting in a blockage of 0.36. The air temperature used was 200 °C. In these simulations initial turbulent kinetic energy of 0.25 J/kg, which is equivalent to turbulence intensity of 5 to 8 per cent was specified. The initial turbulent length scale was taken as ten per cent of the smallest grid.

The Reynolds number for the airflow was 65000 based on equivalent diameter of the duct (=0.133 m) and 18000 based on the outer diameter of the cylinder. This means the flow through the duct was turbulent but that on the front part of the cylinder was laminar.

The two models have significant difference in estimation of turbulent viscosity as shown by the variation of the axial (Fig. 2a) and transversal (Fig. 2b) eddy viscosities with position from the centre of the duct. The flat portion in Figure 2(b) only shows the boundaries of the cylinder itself and has no other physical meaning in this case. As one approaches the solid wall, turbulent eddies approach zero implying that very close to the wall $\nu=\nu_{mol}$. Both 'standard' and RNG k-ε models, however, show the fluid viscosities near solid walls are much larger than the corresponding molecular viscosities. This suggests that turbulence eddies do not die instantaneously on reaching the laminar boundary layer; instead they dampen towards the wall surface. The smaller the turbulent viscosity close to the wall the better is the closure model. As one approaches the separation point the viscosity near the wall deviates even further from the corresponding molecular values. The viscosity peak near the wall is a typical feature of k-ε model - due to overestimation of k. That is the larger the peak the worse is the model.

The discrepancy between molecular and simulated viscosities near the wall is smaller for RNG k-ε model than for the 'standard' k-ε model. Hence RNG k-ε model addresses turbulent behaviour close to the wall more accurately than the 'standard' k-ε model. Moreover, as one approaches the stagnation point, RNG k-ε shows a decreasing tendency in viscosity, which is a better trend (Figure 2(b)) than the one shown by the 'standard' k-ε model.

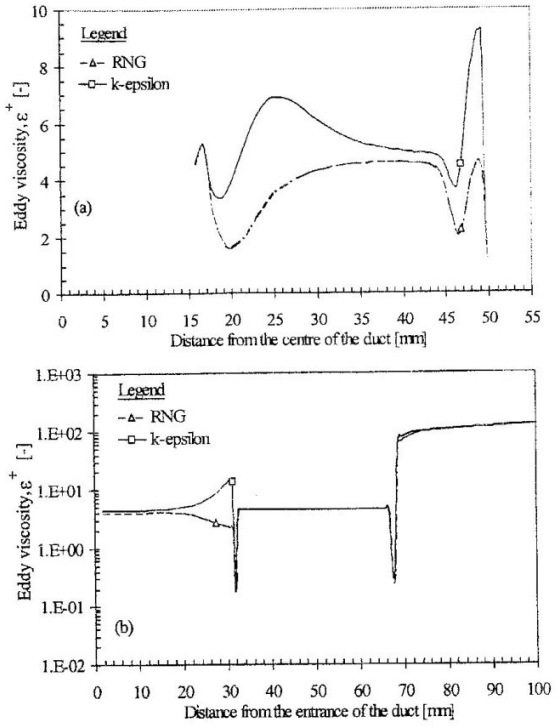

Figure 2. Variation of viscosity along and across the duct (a) y=42.3mm (b) x=0.25 mm

Figure 3 shows the fluid velocity across and along the duct (close to the centre of the cylinder) as obtained using RNG k-ε and 'standard' k-ε models. The region with zero values, in this and subsequent figure, shows the boundaries of the cylinder. These results show that the two models are practically the same close to the cylinder wall. Looking at the velocities close to the stagnation points (front and rear), the two models show significant difference as shown in Figure 4. RNG k-ε model gives a lower value for the stagnation velocity than the 'standard' k-ε model showing that the former gives a better approximation – approaches zero.

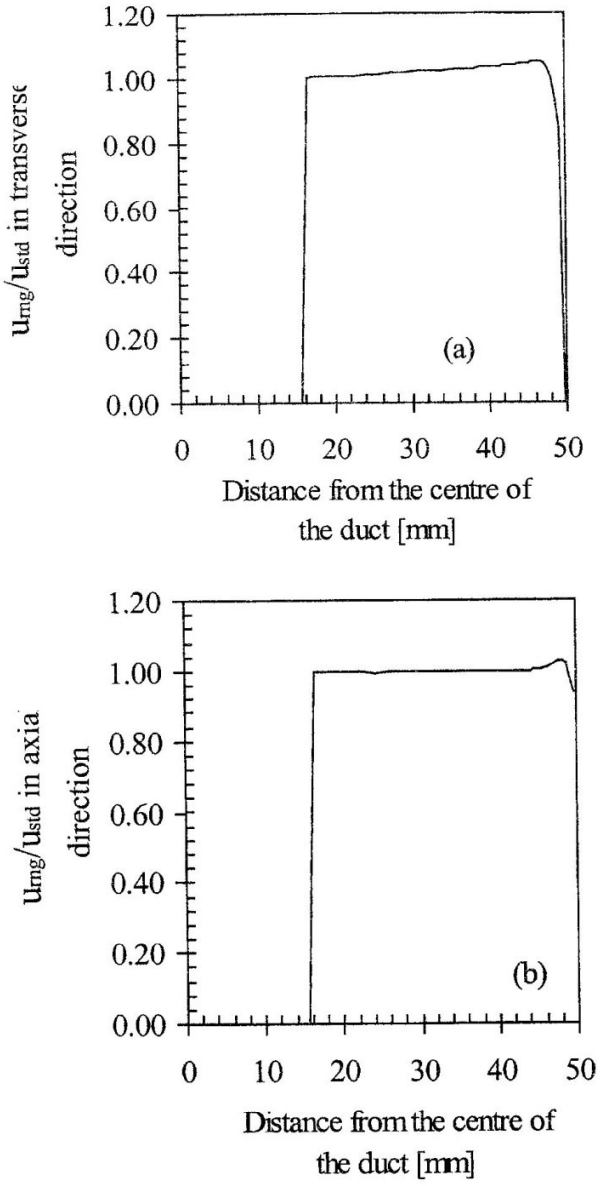

Figure 3. Fluid velocity at different locations across the duct

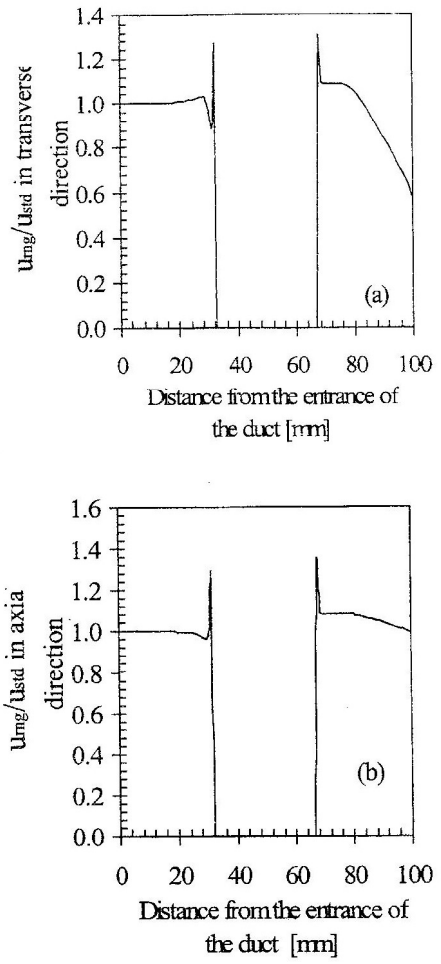

Figure 4. Fluid velocity at different locations along the duct

Because of lack of experimental values, the fluid velocity just outside the boundary layer, obtained from RNG k-ε model was verified by well proven empirical correlation for laminar boundary layer (Equation (11)) as shown in Figure 5. Results from equation (11) with and without blockage are shown to see whether the blockage effect is well addressed by the CFD simulation. The figure shows that the CFD results are in better agreement with empirical results incorporating similar blockage factor. The slight discrepancy between the two curves away from the front stagnation point might be due to inappropriateness of the wall function as the flow begins to separate. Figure 5 also show a strong recirculation after about 120 °.

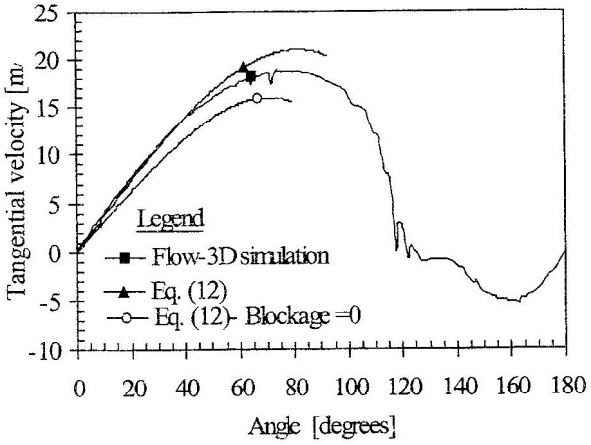

Figure 5. Variation of fluid flow around a cylinder with position (U_o=10 m/s; T_o=200 °C; Blockage=0.36)

The velocity profile, at different locations from the entry point, for flow in the duct upstream of the cylinder was as shown in Figure 6. The figures show a very good agreement between the RNG k-ε simulations with experimental results for Launder and Shima [11] for three-layer model velocity profile (Fig. 6(a)) and with simulation results from Boysan and Patel [12] for turbulent fluctuations (Fig. 6(b)). Therefore, RNG k-ε the model is also suitable for parallel flows.

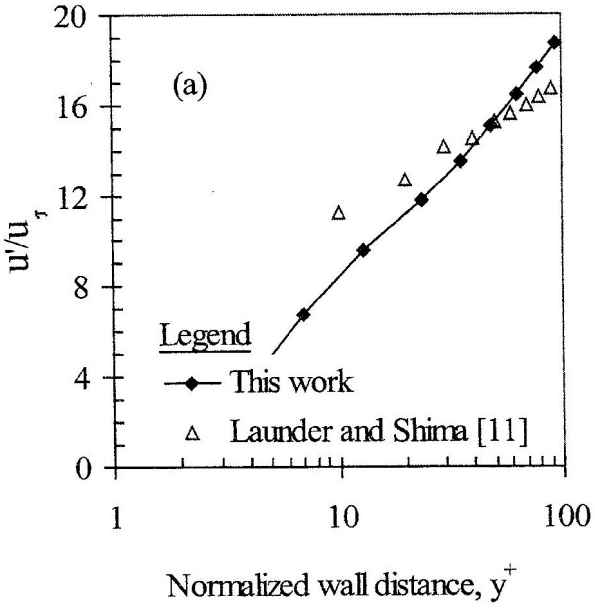

Figure 6 (a)

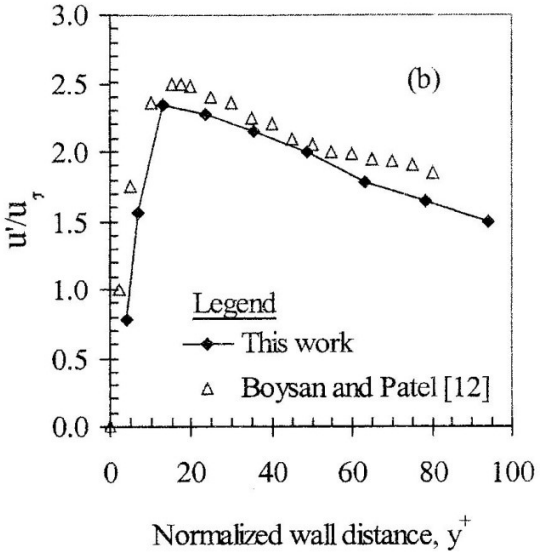

Figure 6(b)

Figure 6. Velocity profile of turbulent flow upstream of the cylinder at different positions from inlet (a) axial velocity (b) transverse velocity

CONCLUSIONS

With the same entry (approach) velocity one could experience different flow patterns in an obstructed duct flow. Whereas the flow in the duct is turbulent and requires turbulent boundary layer theory, the flow around the front part of the cylindrical obstruction is laminar requiring laminar boundary layer theory and that at the back of the cylinder is a complex turbulent flow. Because laminar flow theory is well developed, simulation results for the flow on the front part of the cylinder could be compared with available theory. The tangential velocity just outside the boundary layer as simulated by RNG k-ε model agrees very well with theoretical correlation reflecting the effect of blockage.

Both RNG k-ε and the 'standard' k-ε models require wall functions to take care of the small-scale turbulent eddies.

RNG k-ε model gives a better estimate of k and ε than the 'standard' k-ε model especially in separating and stagnation flows where anisotropy is dominant.

Results obtained from RNG k-ε model for internal flow agrees well with experimental and simulation results available in the literature (Fig. 6).

NOMENCLATURE

Symbol	Description
a_1, a_2, a_3	Constants in Eq. (12)
b_f	Channel blockage factor (= D/H)
$C_{\varepsilon 1}$, $C_{\varepsilon 2}$ C_μ	Constants in turbulence model
D	Outer tube (cylinder) diameter (m)
g	Gravitational acceleration(m/s^2)
H	Channel height (m)
k	Turbulent kinetic energy per unit mass (J/kg)
R	Rate of strain term (Eq. (7))
Re	Reynolds number
S^2	Magnitude of the rate of strain ($= 2S_{ij}S_{ij}$)
S_{ij}	Rate of strain
t	Time (s)
u′	Fluctuating component of velocity (m/s)
u	Fluid velocity component (m/s)
u_∞	Velocity of approach (m/s)
u^*	Shear velocity (m/s)
$\overline{u}$	Mean velocity (m/s)
x'	Arc length measured from the front stagnation point (m)
x, y, z	Cartesian coordinates
y'	Perpendicular distance from the wall m)
y^+	Dimensionless wall distance $\left(= y \cdot u^*/\nu\right)$

Greek symbols

α	Inverse turbulent Prandtl number
δ	Hydrodynamic boundary layer thickness (m)
ε	Turbulent dissipation rate
ε^+	Dimensionless eddy diffusivity
η	Dimensionless distance from the wall (Eq. (11))
η	Variable in Eq. (9)

Λ	Shape factor (Eqs. (11) and (14))
ν	Kinematic viscosity (m^2/s)
ν_{mol}	Molecular kinematic viscosity (m^2/s)
ν_T	Eddy kinematic viscosity (m^2/s)

Superscripts

overbar	Mean value
'	Fluctuating parameters

Subscripts

rng	Based on RNG k-ε model
std'	Based on 'standard' k-ε model

REFERENCES

[1] Williams, P. T. and A. J. Baker, *Numerical Heat Transfer*, Part B: Fund. Vol. 29, no. 2, pp. 137-237 (1996)

[2] Patel, V. C., W. Rodi and G. Scheuerer, *AIAA J.*, vol. 3, no. 9 (1984)

[3] Kondjoyan, A. and D. Daudin, *Int. J. Heat Mass Transfer*, vol. 38, no. 10, pp. 1735 – 1749 (1995)

[4] Li, A.; G. Ahmadi; R. G. Bayer; and M. A. Gaynes, *J. Aerosol Sci.*, vol. 25, no. 1, pp. 91-112 (1994)

[5] Stock, D. E. *Particle dispersion in turbulent gas flows,* Proc. 2nd Int. Conf. Multiphase flow, April 3- 7 1995, Kyoto, Japan, PL2-1- PL2-13 (1995)

[6] Fluent *FLOW-3D, Computational Power Modelling for Scientists and Engineers - Operation manual,* Flow science, Inc., (1993)

[7] Yakhot, V. and L. M. Smith, *J. Scientific Computing*, vol. 7, no. 1, pp. 35-61 (1992)

[8] Schlichting, H. *Boundary - layer theory*, McGraw-Hill Book Co., New York, 1979, 7th Edition.

[9] White, F. *Viscous fluid flow,* McGraw-Hill Book Co., New York, 1974

[10] Zukauskas, A. and J. Ziugzda, *Heat transfer of a cylinder in crossflow,* Hemisphere Publishing Co., Washington, 1985

[11] Launder, B. E. and N. Shima, *AIAA J.*, vol. 27, No. 10 (1989)

[12] Boysan, F. and B. Patel, *Fluent Europe Ltd.* Personal communication. (1998)